

# $\theta$ Vacuum: A Matrix Model

Romuald A. Janik<sup>1,2</sup>, Maciej A. Nowak<sup>2,3</sup>, Gábor Papp<sup>4</sup> and Ismail Zahed<sup>5</sup>

<sup>1</sup> *Service de Physique Théorique, CEA Saclay, F-91191 Gif-Sur-Yvette, France.*

<sup>2</sup> *Department of Physics, Jagellonian University, 30-059 Krakow, Poland.*

<sup>3</sup> *GSI, Planckstr. 1, D-64291 Darmstadt, Germany*

<sup>4</sup> *CNR Department of Physics, KSU, Kent, Ohio 44242, USA &*

*Institute for Theoretical Physics, Eötvös University, Budapest, Hungary*

<sup>5</sup> *Department of Physics and Astronomy, SUNY, Stony Brook, New York 11794, USA.*

We model the effects of a large number of zero modes for  $N_f$  species of quarks at finite vacuum angle  $\theta$ , using a matrix model with gaussian weights constrained by the topological susceptibility and compressibility. The quenched free energy exhibits a cusp at  $\theta < \pi$  that is sensitive to the accuracy of the numerical analysis and the maximum density of winding modes. Our results bear much in common with recent lattice simulations by Schierholtz and others. The unquenched free energy exhibits similar sensitivities, but for small quark masses or a large density of zero modes the results are in agreement with those derived using anomalous Ward identities and effective Lagrangians.

## I. INTRODUCTION

QCD with a finite vacuum angle  $\theta$  is subtle. Canonical quantization [1,2] and variational calculations [3] suggest that the vacuum state depends on  $\theta$ , while covariant quantization seems to indicate otherwise [2]. The issue of the  $\theta$  angle in QCD and the U(1) problem are intertwined [2,4,5]. At finite  $\theta$ , QCD breaks CP. Due to the U(1) anomaly, the  $\theta$  term may be traded from the gauge fields to the quark mass matrix. Bounds from the neutron electric-dipole moment yield  $\theta \leq 10^{-9}$  [6].

In QCD the dependence of the vacuum partition function on the  $\theta$  angle involves an understanding of the vacuum physics which is essentially nonperturbative. First principle calculations are limited and difficult. The reason is that most lattice QCD simulations rely on important samplings by Monte Carlo techniques which require positivity of the action configuration by configuration. At finite  $\theta$  the action is complex in Euclidean space.

Lattice simulations using  $CP^n$  models as well as Yang-Mills theories [7–9] have been recently carried out, with somehow opposite conclusions. A number of effective models have been used to gain insights to this important problem [10–12], including recent conjectures [13]. Unfortunately the conventional lore of power counting, such as chiral perturbation theory, becomes subtle at finite  $\theta$  [2,14], although some exact constraints can still be inferred from Ward identities [2,?,5].

In this paper, we will assume that the vacuum supports a  $\theta$  angle and proceed to analyze some related issues using a matrix model. The main thrust of our investigation is to try to find out the conditions under which a numerical analysis of this problem (albeit in a model) compares to analytical or quasi-analytical solutions. In sections 2 and 3 we introduce the model, and discuss the quenched case. The free energy is found to depend sensitively on the maximum density of winding modes <sup>1</sup>  $\mathbf{n}$  and the accuracy of the numerical calculations. Our observations are similar (although not identical) to those reached recently by Schierholtz and others [7–9] using lattice simulations. In section 4, we discuss the unquenched case and show that under general conditions the saddle-point results agree with the numerical calculations. Our conclusions are in section 5. Some technical details are given in the Appendices.

## II. MATRIX MODEL

Consider the partition function described by

---

<sup>1</sup>In the unquenched case the number of winding modes is the number of zero modes.

$$Z(\theta, N_f) = \left\langle \prod_{j=1}^{N_f} \det \begin{pmatrix} im_j e^{i\theta/N_f} & W \\ W^\dagger & im_j e^{-i\theta/N_f} \end{pmatrix} \right\rangle. \quad (1)$$

where the averaging is carried using the weight

$$\sum_{n_\pm} \int dW dW^\dagger e^{-\frac{1}{2} n \text{Tr} W^\dagger W} e^{\frac{-\chi^2}{2\chi_* V}} e^{\frac{-\sigma^2}{2\sigma_* V}}. \quad (2)$$

Here  $W$  is a complex hermitian asymmetric  $n_+ \times n_-$  matrix,  $n = n_+ + n_-$ , and  $\sigma \pm \chi = 2n_\pm - \langle n \rangle$ . The mean number of zero modes  $\langle n \rangle$  is either fixed from the outside or evaluated using the gaussian measure (2). For simplicity in this paper we used the quenched measure without the fermion determinant to fix  $\langle n \rangle$ . Throughout, the value of the quark condensate  $\Sigma = 1$  in the chiral limit. It is readily reinstated by dimensional inspection.

For a recent review on matrix models in QCD we refer to [15] (and references therein). In short, (1) with gaussian weights is borrowed from the effective instanton vacuum analysis [16] where  $n_+$  counts the number of right-handed zero modes, and  $n_-$  the number of left-handed zero modes (restricted to zero dimension). The number of exact topological zero modes is commensurate with the net winding number carried by the instantons and antiinstantons. By analogy with [16],  $\chi_*$  and  $\sigma_*$  will refer to the unquenched topological susceptibility and particle compressibility, respectively. Higher susceptibilities may be enforced by non-gaussian weights [17,18], provided that the QCD beta function is restricted to its one-loop form. This alternative will be discussed elsewhere.

From [16] we have  $\sigma_*^2 = 4\mathbf{n}_*/b$  with  $b = 11N_c/3$  and  $\mathbf{n}_* = \langle n \rangle/V$  the mean density of zero modes. If the compressibility  $\sigma_*$  is assumed small in units of  $\Sigma = 1$ , then typically  $n \sim \langle n \rangle$ . We note that for the canonical choice  $\mathbf{n}_* = 1$ ,  $\sigma_* = 0.6$  for  $N_c = 3$ . Finally, through a chiral rotation the  $\theta$  angle may be removed from the determinant to generate an extra phase  $e^{i\chi\theta}$  in the measure (see also (11)). In this form, the  $2\pi$  periodicity in  $\theta$  is manifest. We recall that in the original instanton model, CP is explicitly upset at finite  $\theta$ , with the exception of  $\theta = \pm\pi \pmod{2\pi}$ <sup>2</sup>.

### III. $N_F = 0$

In this section we will only analyze the quenched partition function with  $N_f = 0$ , thereby probing the nature of the measure (2). As we will show, this is not a trivial exercise and the outcome bears much in common with current quenched lattice simulations. First, we discuss the case where  $\langle n \rangle = \infty$  with no restriction on the value of  $n$ , and hence no restriction on the value of  $\chi$ . Second, we discuss the case where  $\langle n \rangle$  is large but finite, so that  $|\chi| \leq n$  with typically  $n \sim \langle n \rangle$  for a peaked distribution in  $n$ .

#### A. Infinite Sum

When the sum is unrestricted and infinite, we have for the quenched partition function (up to an irrelevant normalization)

$$Z_Q(\theta) = Z(\theta, 0) = \sum_{\chi=-\infty}^{\infty} e^{i\chi\theta} e^{-\chi^2/2V\chi_*}. \quad (3)$$

Using Poisson resummation formula we have

$$Z_Q(\theta) = \sum_{k=-\infty}^{+\infty} e^{-\frac{1}{2}V\chi_*(\theta-2\pi k)^2} = \theta_3(\theta/2, e^{-\tau}). \quad (4)$$

where the last equality involves the third elliptic  $\theta$ -function with  $\tau = 1/(2V\chi_*)$ . The result is manifestly  $2\pi$  periodic. The vacuum free energy,  $F_Q(\theta) = -\ln Z_Q(\theta)/V$  as  $V \rightarrow \infty$  is simply

---

<sup>2</sup>Under CP  $\theta = \pi$  goes to  $-\pi$  which is the same as  $\pi$  because of the  $2\pi$  periodicity. Multiple degeneracy of states can however take place [5,11,12].

$$F_Q(\theta) = \min \frac{1}{2} \chi_* (\theta + \text{mod } 2\pi)^2 \quad (5)$$

in agreement with the saddle-point approximation to (3). This simple result is the same as the one obtained using large  $N_c$  arguments [11], and recent duality arguments [13]. We observe that the cusp at  $\theta = \pi \pmod{2\pi}$  sets in for  $V = \infty$ . For finite  $V$  the sums converge uniformly, so that

$$F'_Q(\theta) = -\frac{2}{V Z_Q(\theta)} \sum_{\chi=1}^{\infty} \chi \sin(\chi\theta) e^{-\chi^2/2V\chi_*} \quad (6)$$

which is always zero at  $\theta = \pi$ . As  $V \rightarrow \infty$ , the interchange of the derivative with the sum is not valid, hence the cusps. When translated to the quenched instanton calculations, these cusps indicate a new phase with spontaneous CP violation. A similar observation was made in the context of 1+1 compact electromagnetism using the character expansion [19].

Finally, we note that (4) can also be rewritten as

$$Z_Q(\theta) = Z_E(\theta) + Z_O(\theta) = \frac{1}{2} \sqrt{\frac{\pi}{\tau}} \left( \sum_{k=-\infty}^{+\infty} e^{-\frac{1}{4\tau}(\theta - k\pi)^2} + \sum_{k=-\infty}^{+\infty} (-1)^k e^{-\frac{1}{4\tau}(\theta - k\pi)^2} \right) = \theta_3(\theta, e^{-4\tau}) + \theta_2(\theta, e^{-4\tau}) \quad (7)$$

where  $Z_E$  is  $\pi$  periodic and  $Z_O$  is  $\pi$  antiperiodic. The appearance of  $(-1)^k$  in the second sum in (7) is important for restoring the  $2\pi$  periodicity in the full sum. In the thermodynamical limit, the even and odd sums are dominated by single Gaussians with  $F_E = \chi_* (\theta - k\pi)^2/2$  for  $|\theta/\pi - k| \leq 1/2$ , and  $F_O = F_E + ik\pi/V$ .

## B. Finite Sum

In the model we are considering the sum over  $\chi$  is restricted to  $|\chi| < N$ , with  $N = \max n$ . We will denote by  $\mathbf{n} = N/V$  the maximum density of winding modes. While in general  $\mathbf{n} \neq \mathbf{n}_*$ , for a peaked distribution in  $n$  (small compressibility  $\sigma_*$ ) we expect  $\mathbf{n} \sim \mathbf{n}_*$ . This will be assumed throughout unless indicated otherwise. Hence

$$Z_Q(\theta) = \sum_{\chi=-(N-1)}^{N-1} e^{i\theta\chi} e^{-\chi^2/2V\chi_*} \quad (8)$$

Approximating the sum in (8) by an integral and evaluating it by saddle point we obtain  $Z_Q \sim e^{-V\chi_*\theta^2/2}$ .

In Fig. 1 we show the numerically generated result versus the saddle point approximation for the full free energy ( $2\pi$ -periodic) and different values of  $\mathbf{n}$ . The normalization was chosen so that  $F_Q(0) = 0$ . For  $N = 250$  and  $\chi_* = 1$ , the double precision (16 digit) numerics (circles) breaks away from the saddle point approximation (solid line) at  $\theta/\pi \sim 0.2$  for both  $\mathbf{n} = 1$  and  $\mathbf{n} = 4$ , while the high-precision [20] (64 digits) calculations (dashed line) break away at  $\theta/\pi \sim 0.3$  at  $\mathbf{n} = 1$  but agree with the saddle point result at  $\mathbf{n} = 4$ .

The leveling for small values of  $\mathbf{n}$  persists even at infinite accuracy, and in our case is caused by the finite range of the summation over  $\chi$  in (8). Indeed, using the Euler-MacLaurin summation formula, we have

$$\sum_{\chi=0}^{N-1} f(\chi) - \int_0^N f(\chi) d\chi = -\frac{1}{2}[f(0) + f(N)] + \frac{1}{12}[f'(N) - f'(0)] - \frac{1}{720}[f'''(N) - f'''(0)] + \dots \quad (9)$$

where  $\dots$  stand for odd derivatives of  $f(N) = 2 \cos(N\theta) e^{-N^2/2V\chi_*}$ . The generic behavior of the correction terms is a non-exponential prefactor times  $e^{-N^2/2\chi_*V}$  with no dependence on  $\theta$ <sup>3</sup>. This should be compared to the leading order result,  $e^{-V\chi_*\theta^2/2}$ , hence, a breakdown of the saddle-point approximation for  $N = V$  is expected at  $\chi_*\theta^2 \sim 1/\chi_*$ , that is  $\theta/\pi \sim 1/\chi_*\pi \approx 0.3$ , in agreement with the high-precision calculations of Fig. 1.

If we were to increase the density of winding modes to  $\mathbf{n} \geq \pi\chi_*$ , then for say  $\mathbf{n} = 4$ , the saddle-point result is recovered as indicated by the stars (Fig. 1). The breaking point noticed above, now lies outside the period of the free energy (at  $\theta \sim \mathbf{n}/\chi_*$ ). Again, the precision in the numerical calculation is important. For  $\mathbf{n} = 4$  the precision is upgraded from 100 digits for  $\theta/\pi < 0.3$  to 150 digits for  $\theta/\pi > 0.3$ . We have observed that for low precision measurements (16 digits), the numerical calculations deviate from the saddle-point approximation for small values of  $\theta/\pi \sim 0.2$  (circles) even for  $\mathbf{n} = 4$ .

<sup>3</sup> $\theta$  enters only in the prefactor which drops when taking the logarithm and dividing out by  $V$ .

### C. Comparison to Lattice Simulations

The observations of the preceding paragraph may be summarized as follows: the leveling of the quenched free energy of the matrix model as a function of  $\theta$  is sensitive to the numerical accuracy of the calculation. The leveling stabilizes at large numerical accuracy, and is found to depend on the maximum density of winding modes  $\mathbf{n}$  (typically  $\mathbf{n} \sim \mathbf{n}_*$ ) and its relative magnitude to the topological susceptibility. For the measure (2), the leveling occurs at  $\theta_* \sim \mathbf{n}/\chi_*$  in agreement with analytical estimates.

In an interesting series of investigations, Schierholtz [7] analyzed numerically the effects of a finite  $\theta$  angle using a  $CP^3$  model in two-dimensions, and also Yang-Mills theory in four-dimensions. The  $CP^3$  simulations shown in Fig. 2 (left) indicate a leveling of the free-energy for  $\theta \leq \pi/2$ , cautiously interpreted as a possible evidence for a first order transition to a CP-symmetric state [7]. We note the striking similarity of this Figure with Fig. 1.

These findings were recently reexamined by Plefka and Samuel [8] who concluded that the apparent first order transition was a possible artifact of the accuracy of the numerical simulation for fixed lattice size, as shown in Fig. 2 (right). Our findings in the matrix model confirm this observation. The larger the volume  $V$ , the more precision is needed (exponential precision for infinite  $V$ ), due to large cancellations in the partition function caused by the oscillating phase  $e^{i\chi\theta}$ . However, we have also found that the leveling depends quantitatively on the maximum density of winding modes  $\mathbf{n}$  and persists whatever the precision for  $\mathbf{n} \sim 1$ . In this sense, it would be very useful to understand the dependence of the results in [7,8] on  $\mathbf{n}$ , with in particular the ones shown in Fig. 2.

### IV. $N_F > 0$

To assess the effects of light quarks on the partition function of the matrix model, we will consider in this section the general case with  $N_f > 0$ . We will evaluate the free energy of the matrix model in the saddle-point approximation after bosonization, and compare the outcome to direct numerical calculations using large ensemble of asymmetric matrices or quasi-analytical methods.

#### A. Bosonization

In (1) the fermion determinant can be rewritten as an integral over  $N_f n$ -component Grassmanians  $\psi = (\psi_R, \psi_L)$  with dimensions  $(n_+, n_-)$ , that is

$$\det_F = \int d\psi d\psi^\dagger e^{\psi_R^\dagger m e^{i\theta/N_f} \psi_R + \psi_R^\dagger iW \psi_L + L \leftrightarrow R}. \quad (10)$$

The  $\theta$  angle can then be removed from the action by a U(1) transformation  $\psi \rightarrow e^{i\gamma_5\theta/2N_f} q$  with  $\gamma_5 = \text{diag}(\mathbf{1}_{n_+}, -\mathbf{1}_{n_-})$ . The Jacobian of this transformation is just

$$\det_F e^{i\gamma_5\theta/N_f} = e^{i\theta(n_+ - n_-)} \quad (11)$$

which is the well known trade-off through the U(1) anomaly. As a result, we have the following Ward identity

$$\langle n_+ - n_- \rangle_\theta = m \langle q^\dagger i\gamma_5 q \rangle_\theta. \quad (12)$$

Assuming that the range of resummation over  $\chi = n_+ - n_-$  is infinite, that the distribution in  $n = n_+ + n_-$  is peaked ( $n \rightarrow \langle n \rangle$ ) and trading the  $\chi$ -sum by an integral in (1), we have,

$$Z(\theta, N_f) = \int dP dP^\dagger \exp \left\{ \langle n \rangle \left[ -\frac{1}{2} \text{Tr} |P|^2 + \frac{1}{2} \text{Tr} \log |z + P|^2 + \frac{\chi_*}{2\mathbf{n}_*} \left( \log \left( \det \frac{z + P}{\bar{z} + P^\dagger} \right)^{\frac{1}{2}} \right)^2 \right] \right\} \quad (13)$$

where  $z = \text{diag} m_j e^{i\theta/N_f}$ . The logarithm in (13) is multivalued and its  $2\pi$  determination will be assumed. In analogy to the quenched case, the approximation of the sum by an integral should be valid for  $\mathbf{n} \sim \mathbf{n}_* > \pi\chi_{top}$ , where we substituted the quenched topological susceptibility  $\chi_*$ , by the unquenched one  $\chi_{top} \leq \chi_*$ . For small masses  $\chi_{top}$  gets screened (see Appendix C).

To keep a tab on the validity of trading the  $\chi$ -sum by an integral, we observe that for  $N_f = 1$  and  $z = m e^{i\theta}$ , an exact form can be reached for

$$Z(\theta, 1) = \langle (z + P)^{n+} (\bar{z} + P^\dagger)^{n-} \rangle \quad (14)$$

followed by the substitution  $P \rightarrow W$  in the measure (2). Here  $P$  is a complex variable. Because of (11), the same partition function can be written as

$$Z(\theta, 1) = \sum_{\chi=-\infty}^{\infty} e^{i\chi\theta} e^{-\chi^2/2V\chi_*} Z_\chi \quad (15)$$

where  $Z_\chi$  is the partition function for fixed asymmetry  $\chi$ . Again for a peaked distribution  $N \sim \langle n \rangle$ , so that

$$Z_\chi = \left(\frac{2}{N}\right)^{\frac{N-\chi+2}{2}} \pi m^\chi e^{-Nm^2/2} \frac{\Gamma\left(\frac{N+\chi+2}{2}\right)}{\Gamma(\chi+1)} {}_1F_1\left(\frac{N+\chi+2}{2}, \chi+1; Nm^2/2\right). \quad (16)$$

where  ${}_1F_1$  is Kummer's (confluent hypergeometric) function. For even  $\chi$ , it reduces to an associated Laguerre polynomial in  $Nm^2$ . We note that for  $N \rightarrow \infty$  with  $Nm$  and  $\chi$  fixed,  $Z_\chi \sim I_\chi(Nm)$  which is the expected generating function for the microscopic sum rules [21].

### B. Saddle-Point Approximation

Without loss of generality, we can set  $P = \text{diag } p_j e^{i(\theta/N_f - \phi_j)}$ , so that the unsubtracted free energy associated to (13) reads

$$F = \frac{\mathbf{n}_*}{2} \sum_{j=1}^{N_f} \left[ p_j^2 - \log(p_j^2 + 2m_j p_j \cos \phi_j + m_j^2) \right] + \frac{\chi_*}{2} \left( \theta + \arg \left( \prod_{j=1}^{N_f} \left( \frac{m_j + p_j e^{-i\phi_j}}{m_j + p_j e^{i\phi_j}} \right) \right)^{\frac{1}{2}} + \text{mod } 2\pi \right)^2. \quad (17)$$

We note that for  $N_f = 0$  (17) reduces to (5). For small masses  $m_j \ll \chi_* \sim p_j \sim 1$  and (17) simplifies to

$$F = \frac{\mathbf{n}_*}{2} \sum_{j=1}^{N_f} \left( p_j^2 - \log p_j^2 - 2\frac{m_j}{p_j} \cos \phi_j \right) + \frac{1}{2} \chi_* \left( \left( \theta - \sum_{j=1}^{N_f} \phi_j + \text{mod } 2\pi \right) + \sum_{j=1}^{N_f} \frac{m_j}{p_j} \sin \phi_j \right)^2 \quad (18)$$

to order  $\mathcal{O}(m^2)$ . The saddle point in the  $p$ 's decouples and gives  $p_j = 1 - m_j/2 \cos \theta + \mathcal{O}(m^2)$ . To the same order, the saddle point in the  $\phi$ 's is

$$\theta = \sum_{j=1}^{N_f} \phi_j + \mathcal{O}(m) \quad \text{and} \quad m_1 \sin \phi_1 = \dots = m_{N_f} \sin \phi_{N_f}. \quad (19)$$

These equations were derived using large  $N_c$  arguments [11,12] and anomalous Ward-identities [5].

For  $N_f = 1$ , we have

$$\phi = \theta + m \left( \frac{\mathbf{n}_*}{\chi_*} - 1 \right) \sin \theta + \mathcal{O}(m^2) \quad (20)$$

for which the subtracted free energy is  $\Delta F = \mathbf{n}_* m (1 - \cos \theta)$ .

For  $N_f = 2$ , we have

$$\sin \phi_{1,2} = \pm \frac{m_{2,1} \sin \theta}{\sqrt{m_1^2 + m_2^2 + 2m_1 m_2 \cos \theta}} \quad (21)$$

and the subtracted free energy now reads

$$\frac{1}{\mathbf{n}_*} \Delta F(\theta) = |m_1 + m_2| - \sqrt{m_1^2 + m_2^2 + 2m_1 m_2 \cos \theta}. \quad (22)$$

For  $m_1 = m_2$  a cusp develops at  $\theta = \pi$ , since  $\Delta F(\theta) = \mathbf{n}_* |m| (1 - |\cos \theta/2|)$ . In this case both numerator and denominator vanish in (21), hence any value of  $\phi_1$  and  $\phi_2$  is allowed provided that  $\phi_1 + \phi_2 = \pi$ . A similar behavior was noted by many [5,11,12,22,23], following the spontaneous breaking of strong CP.

For  $N_f = 3$ , the explicit solutions to (19) are in general involved, thereby making an analytical form for the free energy involved. At  $\theta = \pi$ , however, the analysis simplifies. Using (19) we obtain a trivial solution with one of the  $\phi$ 's being  $\pi$  and the others zero, and a non-trivial one,

$$\cos \phi_3 = \frac{m_3^2 m_1^2 + m_3^2 m_2^2 - m_1^2 m_2^2}{2m_3^2 m_1 m_2} \quad (23)$$

which is doubly degenerate for

$$m_1 m_2 > m_3 |m_1 - m_2|. \quad (24)$$

The trivial solution corresponds to no cusp at  $\theta = \pi$ , while the non-trivial one yields a cusp at  $\theta = \pi$  because of the double degeneracy. Again similar observations were made using effective Lagrangians [11,22,23] and anomalous Ward identities [5], where (24) is known as Dashen's condition [24]. For sufficient flavor breaking (24) is not fulfilled and strong CP is not spontaneously broken. This is the case in nature where  $m_3 \gg m_1, m_2$ .

### C. Numerical Analysis for $N_f = 1$

In Fig. 3 (left) we compare the fixed size results for the free energy with  $\langle n \rangle = 14$  (circle) and  $\langle n \rangle = 100$  (plus) over one period<sup>4</sup>, using single precision (16 digits) numerical calculations for  $m = 0.5, \chi_* = 1$ . The saddle point solution is indicated by the solid line. Increasing the size of the matrices *worsen* the agreement with the saddle-point result (solid line). The reason is that for  $\pi/2$  the integrand in the sum develops alternating signs with large numerical cancellations. The breakdown of the numerical calculation takes place at  $\theta_* \sim -(\ln \epsilon) / (\langle n \rangle \chi_*)$  with  $\epsilon$  the numerical precision. These observations are new as they pertain to the unquenched free energy.

In Fig. 3 (right) we show the same results after averaging over the size of the matrices (with  $\sigma_* = 1$ ), restoring the  $2\pi$  periodicity. Changing the gaussian measure in  $n$  to a uniform one with  $|n - \langle n \rangle| \leq 6$  does not make a noticeable change on the Figure. We compare the low (16 digits, circles) and high (64 digits, boxes) precision calculations for an *averaged* size  $\langle n \rangle = 14$  using an ensemble of 500000 matrices. Large size samplings at large  $\theta$  requires *exponentially* larger precision. Much like the quenched case we observe the same dependence on  $\mathbf{n} \sim \mathbf{n}_*$ , causing a departure from the saddle point results at  $\theta \sim 0.6\pi$  for  $\mathbf{n} = 1$ .

Since the  $\mathbf{n} > 1$  region is unaccessible by direct use of random matrices, we will use the partition function for fixed asymmetry  $Z_\chi$  in (15) in the saddle point approximation and perform the final sum in (15) numerically. We have checked that the saddle-point result agrees with the result obtained by averaging over large ensembles of matrices with fixed  $\chi$  for  $\mathbf{n} = 1$ . We refer to this analysis as quasi-analytical and the results are shown in Fig. 3 (right) for  $\mathbf{n} = 1$  (dotted line) and  $\mathbf{n} = 4$  (dashed line).

For small masses and  $\theta < \pi/2$  the free energy in the saddle-point approximation is  $F(\theta) \sim \mathbf{n}_* m (1 - \cos \theta)$  with no cusp whatever  $\theta$ . For large  $m$  a cusp at  $\theta = \pi$  develops, following the decoupling of the flavor (roughly  $m \sim N_f \chi_*$ ). In Fig. 3 the occurrence of a cusp for  $m = 0.5$  and  $\mathbf{n} = 4$  is an artifact of the quasi-analytical analysis where only the saddle-point in  $\chi$  is retained (see above). Indeed, the numerical results from this procedure are compared with the standard saddle-point approximation (see previous section) in Fig. 4 for  $m = 0.001$  (small mass) and  $\mathbf{n}_* = \mathbf{n} = 1$  ( $\langle n \rangle = N$ ).

We may now ask if a levelling in the free energy occurs for small masses  $m$ . As we wrote in section 4.1 this takes place for  $\mathbf{n} < \pi \chi_{top}$ . However, due to the screening of the topological charge by the fermion determinant for small masses we expect  $\chi_{top} \sim m$  (see Appendix C) so that the levelling is ruled out for reasonable values of  $\mathbf{n}$ . We note that the macroscopic limit is reached only for  $Nm$  large. For  $N = 200$  ( $Nm < 1$ ) many modes are still missing in the sum (15) (dotted line). For  $N = 10^4$  ( $Nm \gg 1$ ) and  $\theta < \pi/2$ , the quasi-analytical procedure (solid) and the saddle-point approximation (dashed) are in agreement.

Finally, we now ask whether the standard saddle point method fails for  $\theta > \pi/2$ , leading possibly to a cusp at  $\theta \leq \pi$ , contrary to expectations. For  $N_f = 1$  we can calculate the fixed asymmetry partition function exactly (16) and use it for a comparison with the quasi-analytical procedure (see above). The outcome confirms the standard saddle

<sup>4</sup>Since  $\langle n \rangle$  is fixed even, the periodicity is  $\pi$  and not  $2\pi$  as noted in section 3.1.

point result with no cusp at  $\theta = \pi$ , and infirms the quasi-analytical result for large values of  $\theta$ . We conclude that the saddle-point approximation carried prior to the  $\chi$ -resummation is only valid for  $\theta$  small (the  $1/N$  terms at large  $\theta$  are important), while the one carried after the  $\chi$ -resummation is valid whatever  $\theta$ .

We have numerically checked, that most of the present observations carry to  $N_f > 1$ . In particular, a cusp may form in the latter for sufficiently degenerate quark masses, in agreement with the saddle point analysis discussed above.

## V. CONCLUSIONS

We have analyzed the effects of a finite vacuum angle  $\theta$  on the vacuum partition function described by a matrix model, both in the quenched and unquenched approximation. The results are subtle.

In the quenched case, we have found that the free energy exhibits a cusp at finite  $\theta$  that is sensitive to the precision of the numerical analysis. On this point, we are in agreement with the lattice analysis [8]. However, we have further noticed that the results are also sensitive to the maximum density of winding modes  $\mathbf{n}$ . For a small compressibility or a peaked distribution in  $n$ ,  $\mathbf{n}$  is similar to  $\mathbf{n}_*$ , the mean winding density. For large enough  $\mathbf{n} > 1$  the position of the cusp is moved to  $\theta = \pi$  for high enough precision. This observation may be of relevance to the lattice results [7,8]. In this context, it would be interesting to compare the lattice distributions for  $n_{\pm}$  in [7,8] to the gaussian ones we have used in our work.

In the unquenched case, a similar dependence on  $\mathbf{n}$  is found, where  $\mathbf{n}$  is also interpreted as the maximum density of zero modes. For sufficiently large  $\mathbf{n}$  and large masses the quenched results are recovered. Each mass decouples at  $m \sim \chi_*$ , although for large and degenerate masses  $m \sim N_f \chi_*$  (in units where the quark condensate is one). For  $N_f = 1$  and small masses with  $mV > 1$ , the screening of the topological charge takes place, and the saddle point solution holds without any cusp. For  $N_f = 2, 3$ , the numerical results are found to agree with a saddle-point analysis, and results from anomalous Ward identities and effective Lagrangians. A cusp at  $\theta = \pi$  occurs for sufficiently degenerate quark masses. We have found that the use of the saddle-point approximation at large  $\theta$  requires care.

## ACKNOWLEDGMENTS

We would like to thank G. Shierholtz for discussions and R. Crewther for comments. This work was supported in part by the US DOE grants DE-FG-88ER40388 and DE-FG02-86ER40251, by the Polish Government Project (KBN) grant 2P03B00814 and by the Hungarian grant OTKA-F026622.

## APPENDIX A: ALTERNATIVE SADDLE-POINT WITH $N_F = 1$

An alternative saddle-point analysis can be directly performed for fixed  $\chi$  using representation (15). For that, we define

$$\chi = -in \cdot y. \quad (\text{A1})$$

The solution for the saddle point equations gives

$$\begin{aligned} P_{sp} &= \frac{-m^2 \pm \sqrt{m^4 + 4(m^2 - y^2)}}{2\bar{z}} + \frac{iy}{\bar{z}}, \\ P_{sp}^\dagger &= \frac{-m^2 \pm \sqrt{m^4 + 4(m^2 - y^2)}}{2z} - \frac{iy}{z}. \end{aligned} \quad (\text{A2})$$

For a peaked distribution in  $n$  we expect  $n \sim \langle n \rangle$ . The  $P_{sp}$ 's are related to the condensate by

$$-i\langle q^\dagger q \rangle = \frac{1}{V} \partial_m \log Z = \frac{\mathbf{n}_*}{2} (P_{sp}^\dagger e^{i\theta} + P_{sp} e^{-i\theta}). \quad (\text{A3})$$

The value of  $y$  is fixed by requiring the vanishing of the term proportional to  $\chi$ . Hence, the consistency condition reads

$$\log \frac{D + iy}{D - iy} + 2i\theta + 2i \frac{y\mathbf{n}_*}{\chi_*} = 0 \quad \text{or} \quad \arctan \frac{y}{D} + \theta + \frac{y\mathbf{n}_*}{\chi_*} = 0 \quad (\text{A4})$$

where  $D = (m^2 \pm \sqrt{m^4 + 4(m^2 - y^2)})/2$ , with  $y$  satisfying

$$\langle n_+ - n_- \rangle = \mathbf{n}_* V \frac{m}{2} (P_{sp}^\dagger e^{i\theta} - P_{sp} e^{-i\theta}) = \mathbf{n}_* y. \quad (\text{A5})$$

In the consistency condition, the principal branch of the logarithm is retained, making the saddle-point result manifestly  $2\pi$  periodic in  $\theta$ . We note that the present derivation is equivalent to performing the saddle-point calculation for  $y$  without substituting the form (A2) for  $P_{sp}$ 's. The associated free energy is

$$F = -\frac{1}{V} \log Z(\theta) = -\frac{\mathbf{n}_*}{2} \left( \log \left[ \frac{D^2 + y^2}{m^2} \right] - \frac{1 + y^2}{D^2 + y^2} m^2 - \frac{\mathbf{n}_* y^2}{\chi_*} \right). \quad (\text{A6})$$

The subtracted free energy is  $V \Delta F(\theta) = -\ln Z(\theta)/Z(0)$ .

## APPENDIX B: TOPOLOGICAL DENSITY

The topological density  $\langle n_+ - n_- \rangle$  measures the difference between the number of zero modes with plus and minus charges, in the volume  $V$  fixed by the width of the quenched topological susceptibility  $\chi_*$ . This is also the amount of U(1) charge in the vacuum state thanks to (12). At the saddle point ( $N_f = 1$ )

$$\langle n_+ - n_- \rangle = i \partial_\theta \ln Z(\theta)/V = \mathbf{n}_* V \frac{m}{2} (P_{sp}^\dagger e^{i\theta} - P_{sp} e^{-i\theta}) = \mathbf{n}_* y. \quad (\text{B1})$$

We see that  $y$  measures directly the topological density at the saddle point. For a large mass  $m$

$$y = -\frac{\theta}{\frac{1}{D} + \frac{\mathbf{n}_*}{\chi_*}} \sim -\frac{1}{\mathbf{n}_*} \chi_* \theta \left( 1 - \frac{\chi_*}{\mathbf{n}_* m^2} \right) \quad (\text{B2})$$

while for a small mass  $m$

$$\pm y = -m \tan \theta |\cos \theta| - m^2 \frac{\chi_* - 2\mathbf{n}_*}{4\chi_*} \sin 2\theta + \mathcal{O}(m^3). \quad (\text{B3})$$

The  $\pm$  solutions correspond to the transformation  $\theta \leftrightarrow -\theta$ , whereas the absolute value corresponds to the change of the branch in the solution of the consistency equation.

## APPENDIX C: TOPOLOGICAL SUSCEPTIBILITY

The topological susceptibility measures the variance of  $(n_+ - n_-)$  in the vacuum state at finite  $\theta$ . It is simply  $\chi_{\text{top}} = -\partial y / \partial \theta \mathbf{n}_*$ . In the large mass limit

$$\chi_{\text{top}} = \chi_* \left( 1 - \frac{\chi_*}{\mathbf{n}_* m^2} \right) + \mathcal{O}(m^{-3}), \quad (\text{C1})$$

giving  $\chi_{\text{top}} = \chi_*$  in the quenched case ( $m = \infty$ ). In the small mass limit and  $|\theta| < \pi/2$ ,

$$\chi_{\text{top}} = \mathbf{n}_* m |\cos \theta| + \mathbf{n}_* m^2 \frac{\chi_* - 2\mathbf{n}_*}{2\chi_*} \cos 2\theta + \mathcal{O}(m^3). \quad (\text{C2})$$

For  $\theta > \pi/2$  we have  $\langle (n_+ - n_-)^2 \rangle < 0$ , which is possible since the measure is not semi-definite.

The quark condensate for large masses is

$$-i \langle q^\dagger q \rangle = \frac{\mathbf{n}_*}{m} \left( 1 - \frac{\chi_*^2}{\mathbf{n}_*^2 m^2} \theta^2 \right) \quad (\text{C3})$$

and for small masses is

$$-i \langle q^\dagger q \rangle = \mathbf{n}_* \cos \theta - \mathbf{n}_* m \left( \frac{1}{2} + \frac{\chi_* - 2\mathbf{n}_*}{2\chi_*} \sin^2 \theta \right) + \mathcal{O}(m^2) \quad (\text{C4})$$



The anomalous U(1) Ward identity is given by

$$\chi_{top} = -im\langle q^\dagger q \rangle - m^2 \underbrace{\langle q^\dagger \gamma_5 q q^\dagger \gamma_5 q \rangle}_{\chi_{ps}}. \quad (C5)$$

For small masses, the insertion of (C2-C4) into (C5) yield

$$\chi_{ps} = -\mathbf{n}_* \left( \frac{1}{2} + \frac{\chi_* - 2\mathbf{n}_*}{2\chi_*} \cos^2 \theta \right) \quad (C6)$$

for the pseudoscalar correlator (rightmost term in (C5)). It is finite in the chiral limit. For  $\theta = 0$  we recover the result [25]. For large enough  $\mathbf{n}_* > \chi_*$  at certain finite angles the pseudoscalar correlator becomes zero. For large masses we have  $\chi_{ps} = (\mathbf{n}_* - \chi_*)/m^2$ . The present relations generalize readily to  $N_f > 1$ .

#### APPENDIX D: RESOLVENT FOR FIXED $\chi$

The resolvent for the matrix model considered here reads

$$G(z) = \left\langle \frac{1}{2N} \text{Tr} \frac{1}{z - \begin{pmatrix} ime^{i\theta} & W \\ W^\dagger & ime^{-i\theta} \end{pmatrix}} \right\rangle \quad (D1)$$

Since the overlap matrix elements do not mix different flavors the resolvent splits into a sum of 1-flavor resolvents and we get effectively  $N_f$  copies of the appropriate 1-flavor eigenvalue distributions.

Since the matrix is nonhermitian it turns out that the eigenvalues lie on a curve (more precisely on two intervals - see below). This comes from the decomposition ( $N_f = 1$ )

$$\begin{pmatrix} ime^{i\theta} & W \\ W^\dagger & ime^{-i\theta} \end{pmatrix} = im \cos \theta \mathbf{1} + \begin{pmatrix} -m \sin \theta & W \\ W^\dagger & m \sin \theta \end{pmatrix} \quad (D2)$$

So the eigenvalues are just the eigenvalues of the two-level hermitian chiral system displaced by  $im \cos \theta$ . We will write  $z' = z - im \cos \theta$  and introduce the self energies defined by

$$\left\langle \frac{1}{z - \begin{pmatrix} ime^{i\theta} & W \\ W^\dagger & ime^{-i\theta} \end{pmatrix}} \right\rangle = \begin{pmatrix} \frac{1}{z - \Sigma_1} & 0 \\ 0 & \frac{1}{z - \Sigma_2} \end{pmatrix} \quad (D3)$$

Taking into account the fact that the random matrices are asymmetric, we obtain the following equation for the self-energies

$$\Sigma_1 = \frac{1 - \frac{x}{2}}{z' - m \sin \theta - \Sigma_2} \quad (D4)$$

$$\Sigma_2 = \frac{1 + \frac{x}{2}}{z' + m \sin \theta - \Sigma_1} \quad (D5)$$

with  $x = \chi/N$ . The trace of the resolvent is just  $(\Sigma_1 + \Sigma_2)/2$ . Hence

$$G(z) = z' \cdot \frac{1 - \sqrt{1 - \frac{4}{\sigma} + \frac{x^2}{\sigma^2}}}{2} - \frac{m \sin \theta}{2\sigma} x \quad (D6)$$

where  $\sigma = z'^2 - m^2 \sin^2 \theta$ . The eigenvalues lie on two intervals determined by

$$z'_{cut}{}^2 - m^2 \sin^2 \theta = \frac{x^2}{2 \pm \sqrt{4 - x^2}} \quad (D7)$$

and, for asymmetric matrices, there are additional Dirac delta spikes at  $z = m \sin \theta$  when  $\chi$  is negative and at  $z = -m \sin \theta$  when  $\chi$  is positive. Explicitly the eigenvalue distribution reads ( $\lambda = \lambda_R + i\lambda_I$ )

$$\nu(\lambda) = \delta(\lambda_I - m \cos \theta) \left\{ \chi \delta(\lambda_R + m \sin \theta) + \frac{1}{2\pi} (\lambda_R - m \sin \theta) \sqrt{1 - \frac{4}{\sigma} + \frac{x^2}{\sigma^2}} \right\} \quad (\text{D8})$$

for  $\chi$  positive and

$$\nu(\lambda) = \delta(\lambda_I - m \cos \theta) \left\{ |\chi| \delta(\lambda_R - m \sin \theta) + \frac{1}{2\pi} (\lambda_R - m \sin \theta) \sqrt{1 - \frac{4}{\sigma} + \frac{x^2}{\sigma^2}} \right\} \quad (\text{D9})$$

for  $\chi$  negative. The structure of these distributions is not universal, but may be useful for understanding the  $\theta$  structure from the bulk QCD spectrum using cooled lattice gauge configurations.

- [1] R. Jackiw in *Relativity, Groups and Topology*, Les Houches 1983.
- [2] H. Yamagishi and I. Zahed, hep-ph/9507296, hep-th/9709125.
- [3] B. van den Heuvel and P. van Baal, Nucl. Phys. Proc. Suppl. **42**, 823 (1995).
- [4] R.J. Crewther, Phys. Lett. **B70**, 349 (1977); M.A. Shifman, A.I. Vainshtein and V.I. Zakharov, Nucl. Phys. **B166**, 439 (1980); D.I. Diakonov and M.I. Eides, Sov. Phys. JETP **54**, 232 (1981).
- [5] R.J. Crewther, in *Field Theoretical Methods in Particle Physics*, Ed. W. Rühl, Plenum 1980; R.J. Crewther, Nucl. Phys. **B209** (1982) 413.
- [6] V. Baluni, Phys. Rev. D **19**, 2227 (1979); R. Crewther, P. Di Vecchia, G. Veneziano and E. Witten, Phys. Lett. **B88**, 123 (1979); for a recent review on the strong CP problem, see e.g. R. Peccei, hep-ph/9807514.
- [7] G. Schierholz, Nucl. Phys. Proc. Suppl. **A37**, 203 (1994).
- [8] J. C. Plefka and S. Samuel, Phys. Rev. D **56**, 44 (1997).
- [9] M. Imachi, S. Kanou and H. Yoneyama, hep-lat/9809139.
- [10] C. Rozenzweig, J. Schechter and G. Trahern, Phys. Rev. D **21**, 3388 (1980); P. Natt and R. Arnowitt, Phys. Rev. D **23**, 1789 (1981);
- [11] E. Witten, Annals of Phys. **128**, 363 (1980).
- [12] P. Di Vecchia and G. Veneziano, Nucl. Phys. **B171**, 253 (1980).
- [13] E. Witten, Phys. Rev. Lett. **81**, 2862 (1998).
- [14] H. Leutwyler, Nucl. Phys. Proc. Suppl. **64**, 223 (1998); R. Kaiser and H. Leutwyler, hep-ph/9806336.
- [15] R.A. Janik, M.A. Nowak, G. Papp and I. Zahed, Acta Phys. Pol. **B29**, 3957 (1998), and references therein.
- [16] M.A. Nowak, J.J.M. Verbaarschot and I. Zahed, Phys. Lett. **B228**, 251 (1989).
- [17] I. Halperin and A. Zhitnitsky, Phys. Rev. Lett. **81**, 4071 (1998); Phys. Lett. **B440**, 77 (1998).
- [18] D. Diakonov, M. Polyakov and C. Weiss, Nucl. Phys. **B461**, 539 (1996).
- [19] A.S. Hassan, M. Imachi, N. Tsuzuki and H. Yoneyama, Prog. Theor. Phys. **94**, 861 (1995).
- [20] D.H. Bailey, NASA Ames RNR Technical Report RNR-94-013.
- [21] H. Leutwyler and A. Smilga, Phys. Rev. D **46**, 5607 (1992).
- [22] M. Creutz, Phys. Rev. D **52**, 2951 (1995).
- [23] A.V. Smilga, hep-ph/9805214.
- [24] R. Dashen, Phys. Rev. D **3**, 1879 (1979).
- [25] R.A. Janik, M.A. Nowak, G. Papp and I. Zahed, Nucl. Phys. **B498**, 313 (1997).

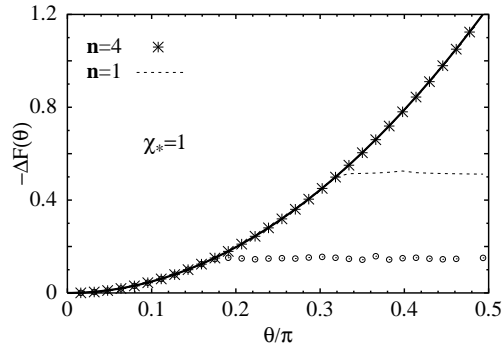


FIG. 1. Quenched free energy  $\Delta F_Q(\theta)$ . See text.

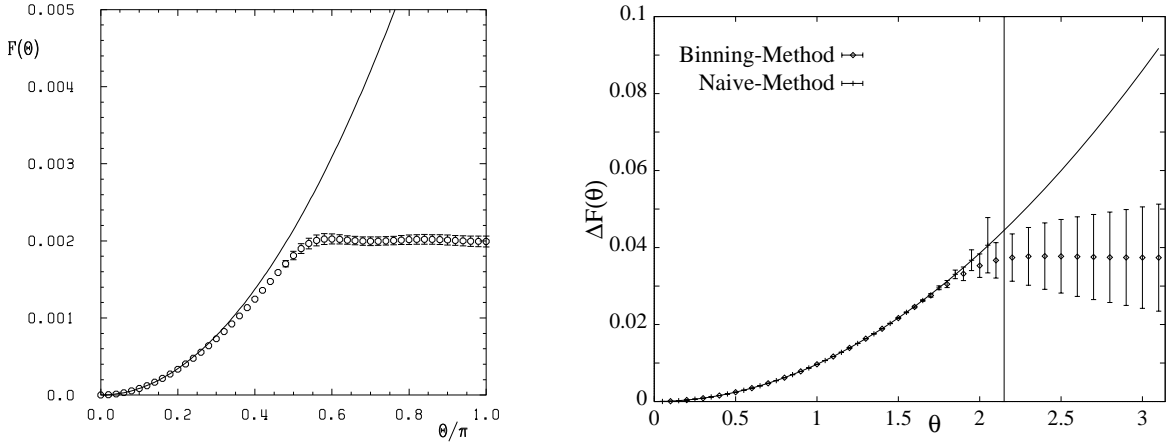


FIG. 2. Free energy from a  $CP^n$  model (left) [7] and (right) [8].

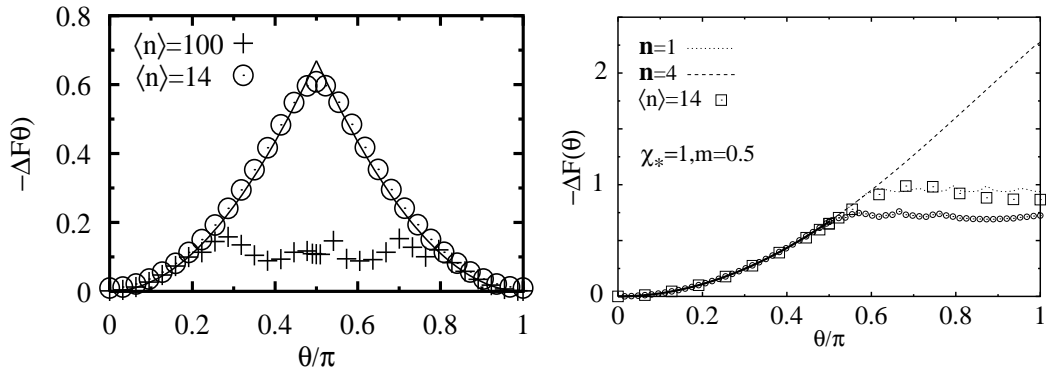


FIG. 3. Unquenched free energy for fixed size matrices (left) and varying size matrices (right) at intermediate mass.

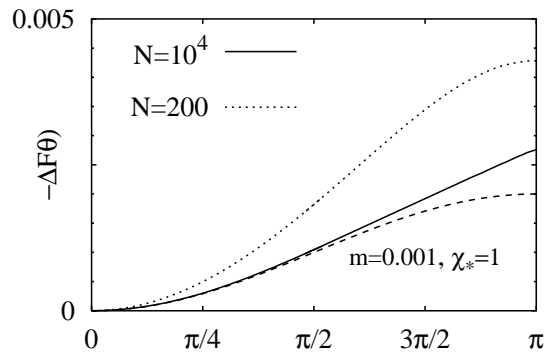


FIG. 4. Unquenched free energy  $\Delta F(\theta)$  for  $N_f = 1$ . See text.